ARTICLE

doi:10.1038/nature12073

Studies of pear-shaped nuclei using accelerated radioactive beams

L. P. Gaffney[1], P. A. Butler[1], M. Scheck[1,2], A. B. Hayes[3], F. Wenander[4], M. Albers[5], B. Bastin[6], C. Bauer[2], A. Blazhev[5], S. Bönig[2], N. Bree[7], J. Cederkäll[8], T. Chupp[9], D. Cline[3], T. E. Cocolios[4], T. Davinson[10], H. De Witte[7], J. Diriken[7,11], T. Grahn[12], A. Herzan[12], M. Huyse[7], D. G. Jenkins[13], D. T. Joss[1], N. Kesteloot[7,11], J. Konki[12], M. Kowalczyk[14], Th. Kröll[2], E. Kwan[15], R. Lutter[16], K. Moschner[5], P. Napiorkowski[14], J. Pakarinen[4,12], M. Pfeiffer[5], D. Radeck[5], P. Reiter[5], K. Reynders[7], S. V. Rigby[1], L. M. Robledo[17], M. Rudigier[5], S. Sambi[7], M. Seidlitz[5], B. Siebeck[5], T. Stora[4], P. Thoele[5], P. Van Duppen[7], M. J. Vermeulen[13], M. von Schmid[2], D. Voulot[4], N. Warr[5], K. Wimmer[18], K. Wrzosek-Lipska[7,14], C. Y. Wu[15] & M. Zielinska[14,19]

There is strong circumstantial evidence that certain heavy, unstable atomic nuclei are 'octupole deformed', that is, distorted into a pear shape. This contrasts with the more prevalent rugby-ball shape of nuclei with reflection-symmetric, quadrupole deformations. The elusive octupole deformed nuclei are of importance for nuclear structure theory, and also in searches for physics beyond the standard model; any measurable electric-dipole moment (a signature of the latter) is expected to be amplified in such nuclei. Here we determine electric octupole transition strengths (a direct measure of octupole correlations) for short-lived isotopes of radon and radium. Coulomb excitation experiments were performed using accelerated beams of heavy, radioactive ions. Our data on ^{220}Rn and ^{224}Ra show clear evidence for stronger octupole deformation in the latter. The results enable discrimination between differing theoretical approaches to octupole correlations, and help to constrain suitable candidates for experimental studies of atomic electric-dipole moments that might reveal extensions to the standard model.

The atomic nucleus is a many-body quantum system, and hence its shape is determined by the number of nucleons present in the nucleus and the interactions between them. For example, nuclei in their ground state in which the proton and neutron shells are completely filled ('doubly magic' nuclei) are spherical. If this configuration is excited, or if more nucleons are added, the long-range correlations between valence nucleons distort the shape from spherical symmetry and the nucleus becomes deformed. In most of these cases, it is well established that the shape assumed has quadrupole deformation with axial and reflection symmetry; that is, the nucleus is shaped like a rugby ball (prolate deformation) or as a discus (oblate deformation). For certain combinations of protons and neutrons, there is also the theoretical expectation that the shape of nuclei can assume octupole deformation, corresponding to reflection asymmetry or a 'pear-shape' in the intrinsic frame, either in a dynamic way (octupole vibrations) or having a static shape (permanent octupole deformation).

Octupole deformation and EDMs

Atoms with octupole-deformed nuclei are very important in the search for permanent atomic electric-dipole moments (EDMs). The observation of a non-zero EDM at the level of contemporary experimental sensitivity would indicate time-reversal (T) or equivalently charge–parity (CP) violation due to physics beyond the standard model. In fact, experimental limits on EDMs provide important constraints on many proposed extensions to the standard model[1,2]. For a neutral atom in its ground state, the Schiff moment (the electric-dipole distribution weighted by radius squared[3]) is the lowest-order observable nuclear moment. Octupole-deformed nuclei with odd nucleon number A ($=Z+N$, see below) will have enhanced nuclear Schiff moments owing to the presence of the large octupole collectivity (spatial correlation between particle states) and the occurrence of nearly degenerate parity doublets that naturally arise if the deformation is static[3–5]. Because a CP-violating Schiff moment induces a contribution to the atomic EDM, the sensitivity of the EDM measurement to CP violation over non-octupole-enhanced systems such as ^{199}Hg (ref. 2), currently providing the most stringent limit for atoms, can be improved by a factor of 100–1,000 (ref. 4). Essential in the interpretation of such limits in terms of new physics is a detailed understanding of the structure of these nuclei. Experimental programmes are in place to measure EDMs in atoms of odd-A Rn and Ra isotopes in the octupole region (see for example, ref. 6) but so far there is little direct information on octupole correlations in these nuclei.

Strong octupole correlations leading to pear shapes can arise when nucleons near the Fermi surface occupy states of opposite parity with orbital and total angular momentum differing by $3\hbar$. This condition is met for proton number $Z \approx 34$, 56 and 88 and neutron number $N \approx 34$, 56, 88 and 134. The largest array of evidence for reflection asymmetry is seen at the values of $Z \approx 88$ and $N \approx 134$, where phenomena such as interleaved positive- and negative-parity rotational bands in even–even nuclei[7], parity doublets in odd-mass nuclei[8], and enhanced electric-dipole (E1) transition moments[9] have been observed. Many theoretical approaches have been developed to describe the observed

[1]Oliver Lodge Laboratory, University of Liverpool, Liverpool L69 7ZE, UK. [2]Institut für Kernphysik, Technische Universität Darmstadt, Darmstadt D-64289, Germany. [3]Department of Physics and Astronomy, University of Rochester, Rochester, New York 14627-0171, USA. [4]ISOLDE, CERN (Organisation Européenne pour la Recherche Nucléaire), Geneva CH-1211, Switzerland. [5]Institut für Kernphysik, Universität zu Köln, Köln D-50937, Germany. [6]GANIL (Grand Accélérateur National d'Ions Lourds), Caen, BP 55027, F-14076, France. [7]Instituut voor Kern- en Stralingsfysica, KU Leuven, Leuven B-3001, Belgium. [8]Department of Nuclear Physics, Lund University, Lund, PO Box 118, 221 00, Sweden. [9]Department of Physics, University of Michigan, Ann Arbor, Michigan 48104, USA. [10]School of Physics & Astronomy, University of Edinburgh, Edinburgh EH9 3JZ, UK. [11]SCK•CEN (Studiecentrum voor Kernenergie - Centre d'Etude de l'énergie Nucléaire), Mol B-2400, Belgium. [12]Department of Physics, University of Jyväskylä, Jyväskylä FI-40014, Finland, and Helsinki Institute of Physics, PO Box 64, FI-00014 Helsinki, Finland. [13]Department of Physics, University of York, York YO10 5DD, UK. [14]Heavy Ion Laboratory, University of Warsaw, Warsaw 02-093, Poland. [15]Physics Division, Lawrence Livermore National Laboratory, Livermore, California 94551, USA. [16]Maier-Leibnitz-Laboratorium, Ludwig-Maximilians-Universität and Technische Universität München, Garching D-85748, Germany. [17]Departamento de Fisica Teorica, Universidad Autónoma de Madrid, Madrid 28049, Spain. [18]Physik Department E12, Technische Universität München, Garching D-85748, Germany. [19]DSM/IRFU/SPhN, CEA Saclay, Gif-sur-Yvette F-91191, France.

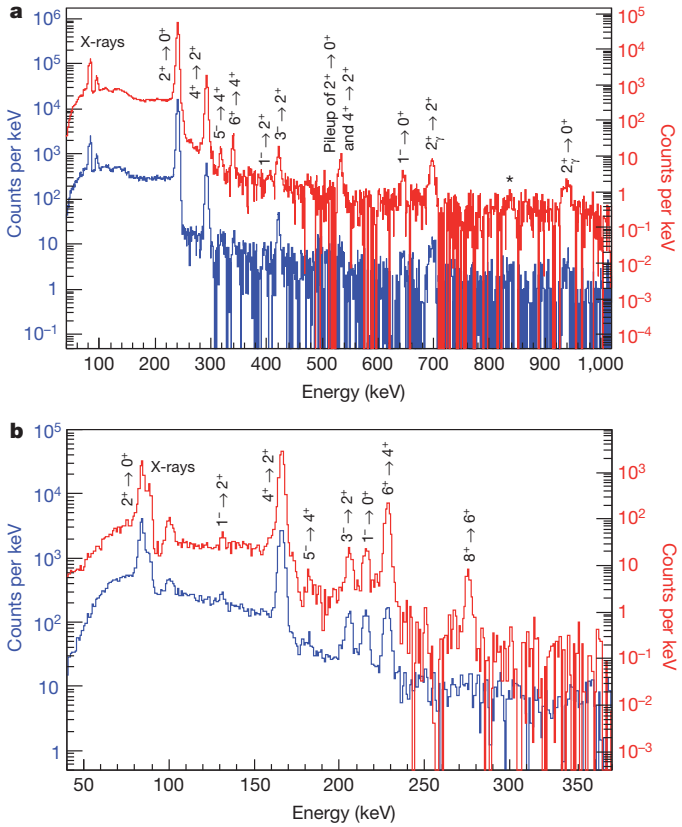

Figure 1 | Representative γ-ray spectra following the bombardment of 2 mg cm^{-2} ^{60}Ni and ^{120}Sn targets by ^{220}Rn and ^{224}Ra. a, ^{60}Ni (blue) and ^{120}Sn (red) bombarded by ^{220}Rn; **b**, targets as **a** but with bombardment by ^{224}Ra. The differences in excitation cross-section for the targets with different Z are apparent for the higher spin states. The γ-rays are corrected for Doppler shift assuming that they are emitted from the scattered projectile. The asterisk in **a** marks an unassigned, 836(2) keV transition. A state at 937.8(8) keV is assigned $I^{\pi} = 2^{+}$ on the basis of its excitation and decay properties; it is assumed to be the bandhead of the γ-band in ^{220}Rn.

experimental features: shell-corrected liquid-drop models[10,11], mean-field approaches using various interactions[12–16], models that assume α-particle clustering in the nucleus[17,18], algebraic models[19] and other semi-phenomenological approaches[20]. A broad overview of the experimental and theoretical evidence for octupole correlations is given in ref. 21.

In order to determine the shape of nuclei, the rotational model can be used to connect the intrinsic deformation, which is not directly observable, to the electric charge moments that arise from the non-spherical charge distribution. For quadrupole deformed nuclei, the typical experimental observables are the electric-quadrupole (E2) transition moments that are related to the matrix elements connecting differing members of rotational bands in these nuclei, and E2 static moments that are related to diagonal matrix elements for a single state. If the nucleus does not change its shape under rotation, both types of moments will vary with angular momentum but can be related to a constant 'intrinsic' moment that characterizes the shape of the nucleus. For pear-shaped nuclei, there will be additionally E1 and electric-octupole (E3) transition moments that connect rotational states having opposite parity. The E1 transitions can be enhanced because of the separation of the centre-of-mass and centre-of-charge. The absolute values of the E1 moments are, however, small ($<10^{-2}$ single particle units) and are dominated by single-particle and cancellation effects[9]. In contrast, the E3 transition moment is collective in behaviour (>10 single particle units) and is insensitive to single-particle effects, as it is generated by coherent contributions arising from the quadrupole-octupole shape. The E3 moment is therefore an observable that should provide direct evidence for enhanced octupole correlations and, for deformed nuclei, can be related to the intrinsic octupole deformation parameters[22]. Until the present measurements, E3 transition moments have been determined for only one nucleus in the $Z \approx 88$, $N \approx 134$ region, ^{226}Ra (ref. 23), so that theoretical calculations of E3 moments in reflection-asymmetric nuclei have not yet been subject to detailed scrutiny.

Experiments and discussion

Coulomb excitation is an important tool for exploring the collective behaviour of deformed nuclei that gives rise to strong enhancement of the probability of transitions between states. Traditionally, this technique has been employed by exciting targets of stable nuclei with accelerated ion beams of stable nuclei at energies below the Coulomb barrier, ensuring that the interaction is purely electromagnetic in character. Whereas E2, E1 and magnetic dipole (M1) transition probabilities dominate in the electromagnetic decay of nuclear states, and hence can be determined from measurements of the lifetimes of the states, E2 and E3 transition moments dominate the Coulomb excitation process allowing these moments to be determined from measurement of the cross-sections of the states, often inferred from the γ-rays that de-excite these levels. In exceptional cases, the Coulomb excitation technique has been applied to radioactive targets like ^{226}Ra, which is sufficiently long-lived (half-life 1,600 yr) to produce a macroscopic sample. It is only comparatively recently that the technique has been extended to the use of accelerated beams of radioactive nuclei such as those from the Radioactive beam EXperimental facility at ISOLDE, CERN (REX-ISOLDE[24]). In the experiments described here,

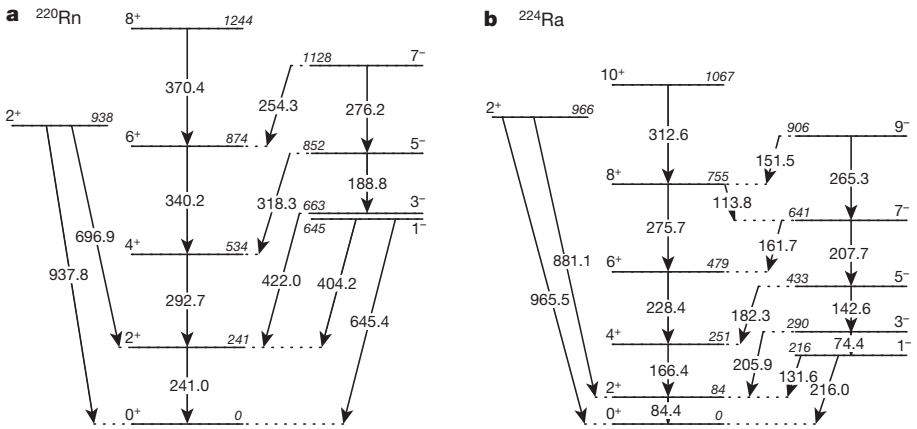

Figure 2 | Partial level-schemes for ^{220}Rn and ^{224}Ra, showing the excited states of interest for this work. a, ^{220}Rn; **b**, ^{224}Ra. Arrows indicate known γ-ray transitions. All energies are in keV (upright font refers to transition energies, italic font refers to state energies) and spins in units of $\hbar$. Note that the level at 938 keV in ^{220}Rn is observed for the first time in this work.

Table 1 | Values of matrix elements measured in the present experiment

Matrix element	^{220}Rn		^{224}Ra	
$<I'\|\|E\lambda\|\|I>$	$\|$m.e.$\|$ (e fm$^{\lambda}$)	$B(E\lambda)\downarrow$ (WU)	$\|$m.e.$\|$ (e fm$^{\lambda}$)	$B(E\lambda)\downarrow$ (WU)
$<0^+\|\|E1\|\|1^->$	<0.10	$<1.5\times10^{-3}$	<0.018	$<5\times10^{-5}$
$<2^+\|\|E1\|\|1^->$	<0.13	$<3\times10^{-3}$	<0.03	$<1.3\times10^{-4}$
$<2^+\|\|E1\|\|3^->$	<0.18	$<2\times10^{-3}$	0.026 ± 0.005	$3.9^{+1.7}_{-1.4}\times10^{-5}$
$<4^+\|\|E1\|\|5^->$	0.028 ± 0.009	$3.0^{+2}_{-1.6}\times10^{-5}$	0.030 ± 0.010	$4^{+3}_{-2}\times10^{-5}$
$<6^+\|\|E1\|\|7^->$	<1.3	<0.5	<0.10	$<3\times10^{-4}$
$<0^+\|\|E2\|\|2^+>$	137 ± 4	48 ± 3	199 ± 3	98 ± 3
$<1^-\|\|E2\|\|3^->$	180 ± 60	60^{+50}_{-30}	230 ± 11	93 ± 9
$<2^+\|\|E2\|\|4^+>$	212 ± 4	63 ± 3	315 ± 6	137 ± 5
$<3^-\|\|E2\|\|5^->$	220 ± 150	60^{+100}_{-50}	410 ± 60	190 ± 60
$<4^+\|\|E2\|\|6^+>$	274 ± 14	73 ± 8	405 ± 15	156 ± 12
$<6^+\|\|E2\|\|8^+>$			500 ± 60	180 ± 60
$<0^+\|\|E2\|\|2^+_\gamma>$	32 ± 7	2.6 ± 1.1	23 ± 4	1.3 ± 0.5
$<0^+\|\|E3\|\|3^->$	810 ± 50	33 ± 4	940 ± 30	42 ± 3
$<2^+\|\|E3\|\|1^->$	<2,600	<760	1,370 ± 140	210 ± 40
$<2^+\|\|E3\|\|3^->$	<5,300	<1,400	<4,000	<600
$<2^+\|\|E3\|\|5^->$	1,700 ± 400	90 ± 50	1,410 ± 190	61 ± 17

The experimental measurements for the absolute values of the matrix elements, $|$m.e.$|$, and the reduced transition probabilities, $B(E\lambda)$, are given here. The values of $B(E\lambda)$ for electromagnetic decay ($\downarrow$) are derived from the matrix elements and are given in single particle units (Weisskopf units, WU). The uncertainties include the 1σ statistical error from the fit (χ^2+1 type) and systematic contributions—beam energy and target thickness uncertainties, deorientation, beam spot effects, and so on. The upper limits correspond to 3σ.

^{220}Rn ($Z=86$, $N=134$) and ^{224}Ra ($Z=88$, $N=136$) ions were produced by spallation in a thick uranium carbide target bombarded by $\sim10^{13}$ protons s^{-1} at 1.4 GeV from the CERN PS Booster. The ions were post-accelerated in REX-ISOLDE to an energy of 2.82 or 2.83 MeV per nucleon and bombarded secondary targets of ^{60}Ni, ^{112}Cd or ^{114}Cd, and ^{120}Sn of thickness approximately 2 mg cm^{-2} with an intensity of about 3×10^5 ions s^{-1} and 7×10^5 ions s^{-1} for Rn and Ra, respectively (Methods). The targets were chosen to give differing electromagnetic excitation (Ni, $Z=28$ versus Sn, $Z=50$; see Fig. 1) and, in the case of Cd, to provide a cross-check to the excitation of a target whose matrix elements are well known and can be measured in these experiments.

The γ-rays emitted following the excitation of the target and projectile nuclei were detected in MINIBALL[25], an array of 24 high-purity germanium detectors, each with six-fold segmentation and arranged in eight triple-clusters. The scattered projectiles and target recoils, distinguished by their differing dependence of energy with angle measured in the laboratory frame-of-reference, were detected in a highly segmented silicon detector[26]. Representative spectra for ^{220}Rn and ^{224}Ra, for which the γ-ray energy is corrected for Doppler shift assuming emission from the scattered projectile, are shown in Fig. 1. Here events were accumulated only if the target recoil was detected in coincidence with γ-rays within a 600-ns time window; these data were corrected for random events. The energy level schemes for ^{220}Rn and ^{224}Ra are shown in Fig. 2.

The spectra reveal strong population of the ground-state band of positive-parity states, excited by direct and multiple E2 Coulomb excitation, and substantial population of the octupole band of negative-parity states, excited by E3 excitation. The yields of the observed γ-ray transitions detected in MINIBALL were measured for two ranges of recoil angles of the target nucleus (28°–38° and 38°–52° for ^{220}Rn; 24°–40° and 40°–54° for ^{224}Ra) for each of the three targets, and combined with existing spectroscopic data (lifetimes of low-lying states[27,28] and their γ-ray branching ratios[7,29,30]) to provide input to the Coulomb-excitation analysis code GOSIA[31] (Methods). The separation of angular ranges increased sensitivity in the measurement by varying the relative excitation probabilities. For ^{220}Rn, 34 independent data points determined 22 free parameters (16 matrix elements and 1 normalization constant for each combination of target and recoil angle range) whereas for ^{224}Ra, 57 data points determined 23 free parameters (17 matrix elements). The analysis was also carried out for ^{220}Rn independently of the previously measured lifetime of the $I^\pi=2^+$ state (τ_{2+})[27], and for ^{224}Ra independently of τ_{4+} (ref. 28); here I is the total angular

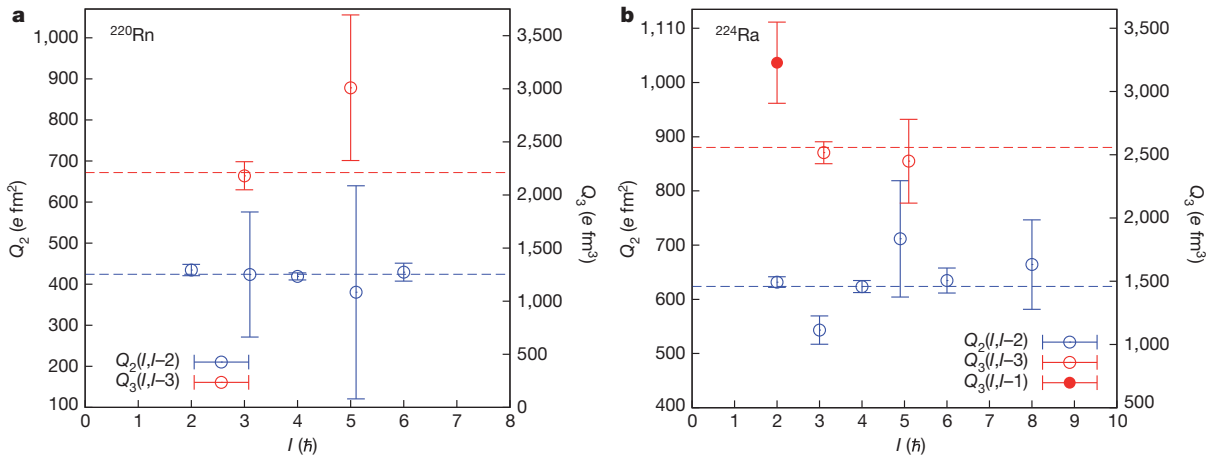

Figure 3 | The values of the E2 and E3 intrinsic moments, $Q_\lambda(I, I')$. **a**, **b**, These values are derived from the matrix elements using the relation $\langle I'||E\lambda||I\rangle=\sqrt{(2I'+1)(2\lambda+1)/16\pi}(I'0\lambda0|I0)Q_\lambda$ for ^{220}Rn (**a**) and ^{224}Ra (**b**). Here $\langle I'||E\lambda||I\rangle$ is the matrix element between states of angular momenta I and I' defined in the text and $(I'0\lambda0|I0)$ is a Clebsch-Gordon coefficient. The dashed lines have the value of the weighted mean for each Q_λ, the error bars are ±1s.d.

Table 2 | The values of the E2 and E3 intrinsic moments, Q_λ

Q_λ	Nucleus						
	^{208}Pb	^{220}Rn	^{224}Ra	^{226}Ra	^{230}Th	^{232}Th	^{234}U
Q_2 (e fm^2)	179 ± 4 (ref. 44)	434 ± 14	632 ± 10	717 ± 3 (ref. 23)	900 ± 6 (ref. 45)	932 ± 5 (ref. 46)	1,047 ± 5 (ref. 45)
Q_3 (e fm^3)	2,100 ± 20 (ref. 44)	2,180 ± 130	2,520 ± 90	2,890 ± 80 (ref. 23)	2140 ± 100 (ref. 47)	1970 ± 100 (ref. 48)	2,060 ± 120 (ref. 47)

Values of Q_λ given here are derived from the matrix elements (see Fig. 3 legend) connecting the lowest-lying states in nuclei near $Z = 88$ and $N = 134$. The values for ^{220}Rn and ^{224}Ra are taken from the present work.

momentum of the state and π is its parity. (For ^{224}Ra the previously measured value of τ_{2+} cannot be determined independently as the $2^+ \rightarrow 0^+$ transition is contaminated with the Ra X-rays.) In both cases the fitted matrix elements for the $2^+ \rightarrow 0^+$ E2 transition (^{220}Rn) and for the $4^+ \rightarrow 2^+$ E2 transition (^{224}Ra) were found to agree, within the experimental uncertainties, with the values obtained using the lifetime measurements.

The measured E1, E2 and E3 matrix elements for ^{220}Rn and ^{224}Ra are given in Table 1. The values of the intrinsic moments, Q_λ, are given in Fig. 3. These are determined from the experimental values of the reduced matrix element between two states having angular momenta I and I' induced to undergo a transition by the electromagnetic operator Eλ, $<I'||\mathrm{E}\lambda||I>$, assuming the validity of the rotational model[22]. Here $\lambda = 1,2,3$ refers to E1, E2, E3 respectively. For the E2 and E3 matrix elements, the measured values are all consistent with the geo metric predictions expected from a rotating, deformed distribution of electric charge, although these data do not distinguish whether the negative-parity states arise from the projection of a quadrupole-octupole deformed shape or from an octupole oscillation of a quadrupole shape[32]. Table 2 compares the experimental values of Q_λ derived from the matrix elements connecting the lowest states for nuclei near $Z = 88$ and $N = 134$ measured by Coulomb excitation. It is striking that while the E2 moment increases by a factor of 6 between ^{208}Pb and ^{234}U, the E3 moment changes by only 50% in the entire mass region. Nevertheless, the larger Q_3 values for ^{224}Ra and ^{226}Ra indicate an enhancement in octupole collectivity that is consistent with an onset of octupole deformation inthis mass region. On the other hand, ^{220}Rn has similar octupole strength to ^{208}Pb, ^{230,232}Th and ^{234}U, consistent with it being an octu pole vibrator. In the case of a vibrator, the coupling of an octupole phonon to the ground state rotational band will give zero values for matrix elements such as $<1^-||\mathrm{E3}||4^+>$, because an aligned octupole phonon would couple the 4^+ state to a 7^- state. Although the present experiment does not have sensitivity to this quantity, this effect has been observed for ^{148}Nd in the $Z \approx 56$, $N \approx 88$ octupole region[33], while for ^{226}Ra the intrinsic moment derived from the measured $<1^-||\mathrm{E3}||4^+>$ is similar to that derived from the value of $<0^+||\mathrm{E3}||3^->$ (ref. 23). The deduced shapes of ^{220}Rn and ^{224}Ra are presented in Fig. 4. Here the values of quadrupole and octupole deformation β_2 and β_3 were extracted from the dependence of the measured Q_2 and Q_3 on the generalized nuclear shape[34].

The conclusions drawn from the present measurements are also consistent with suggestions from the systematic studies of energy levels[7] (relative alignment of the negative-parity band to the positive-parity band) that the even–even isotopes $^{218-222}$Rn and ^{220}Ra have vibrational behaviour while $^{222-228}$Ra have octupole-deformed character (see figures 12 and 13 in ref. 7). For odd-mass ^{219}Rn there is no evidence[35] for parity doubling, whereas for ^{221}Ra a parity doublet of states with $I = 5/2$ separated by 103.6 keV has been observed[36]. In the Ba–Nd region with $Z \approx 56$ and $N \approx 88$, where the octupole states arise from vibrational coupling to the ground-state band, the evidence for parity doubling of the ground state arising from reflection asymmetry is inconclusive[37,38]. This suggests that the parity doubling condition that leads to enhancement of the Schiff moment[15] is unlikely to be met in ^{219,221}Rn. On the other hand ^{223,225}Ra, having parity doublets separated by ~50 keV (ref. 21), will have large enhancement of their Schiff moments.

The values of Q_λ, deduced from the measured transition matrix elements, are plotted in Fig. 5 as a function of N. The anomalously low value of Q_1 for ^{224}Ra, measured here for the first time, has been noted elsewhere[9,13,39]. The measured Q_1 and Q_2 values are in good agreement with recent theoretical calculations of the generator-coordinate extension of the Gogny Hartree–Fock–Bogoliubov (HFB) self-consistent mean field theory[16], particularly using the D1M parameterization[40]. However, as remarked earlier, the trend of the experimental data is that the values of Q_3 decrease from a peak near ^{226}Ra with decreasing N (or A), which is in marked contrast to the predictions of the cluster model calculations[17]. It is also at variance with the Gogny HFB mean-field predictions of a maximum for ^{224}Ra (ref. 16). It should be noted, however, that relativistic mean field calculations[14] predict that the maximum value of Q_3 occurs for radium isotopes between $A = 226$ and 230, depending on the parameterization, and Skyrme Hartree–Fock calculations[15] predict that ^{226}Ra has the largest octupole deformation. Both predictions are consistent with our data. We cannot completely eliminate the possibility that there are unobserved couplings from the ground state to higher-lying 3^- states that should be added (without energy weighting) to the observed coupling to the

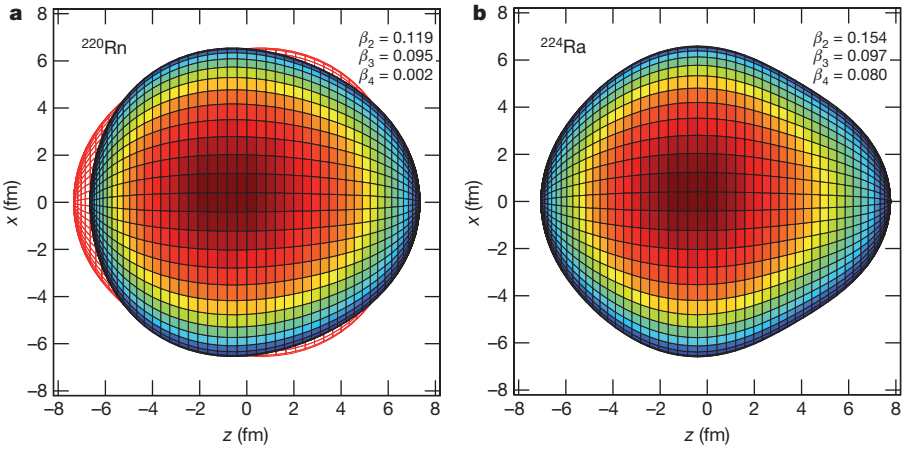

Figure 4 | Graphical representation of the shapes of ^{220}Rn and ^{224}Ra. **a**, ^{220}Rn; **b**, ^{224}Ra. Panel **a** depicts vibrational motion about symmetry between the surface shown and the red outline, whereas **b** depicts static deformation in the intrinsic frame. Theoretical values of β_4 are taken from ref. 10. The colour scale, blue to red, represents the y-values of the surface. The nuclear shape does not change under rotation about the z axis.

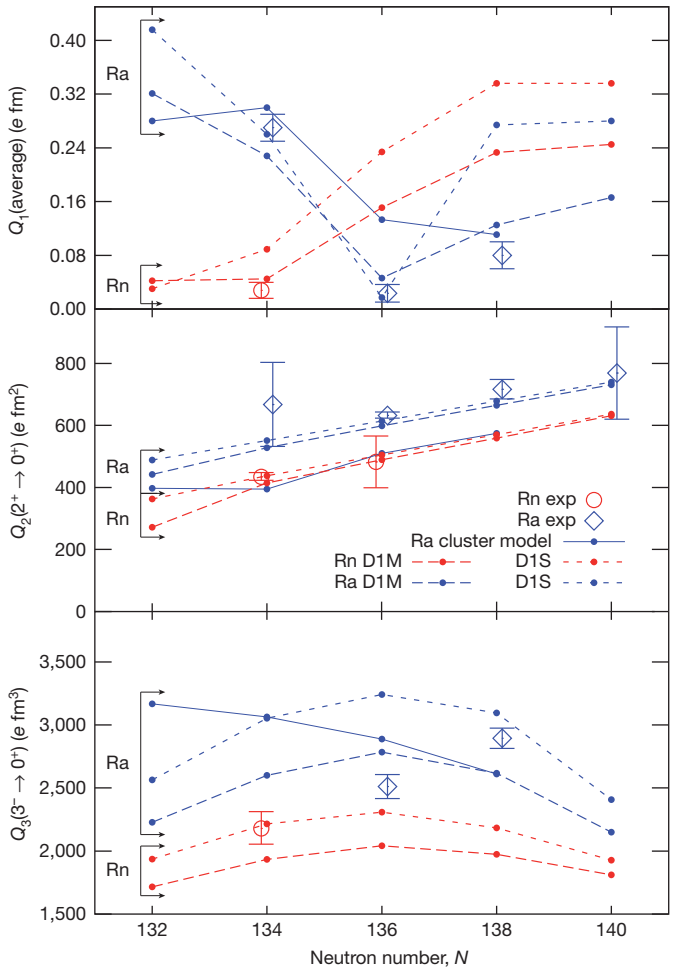

Figure 5 | Values of Q_λ for low-lying transitions in nuclei as a function of N. Measured values for $\lambda \rightarrow 0$ transitions are used for $\lambda = 2, 3$; for $\lambda = 1$ an average value over the measured spin range ($\leq 5\hbar$) is used. Comparisons are made to the theoretical predictions of a cluster model[17] ('Ra cluster model') and mean-field calculations[16] (with two different parameterizations D1M and D1S[40], 'Rn D1M, D1S' and 'Ra D1M, D1S'). The points are connected by lines as a guide to the eye. The experimental data for Rn and Ra isotopes are denoted 'Rn exp' and 'Ra exp' respectively; the data for ^{220}Rn ($N = 134$) and ^{224}Ra ($N = 136$) are from the present work, other data are taken from refs 23, 49 and 50. The error bars are $\pm$1s.d.

lowest 3^- state. However, in a detailed study[33] of octupole strength in ^{148}Nd, where these states lie closer in energy to the lowest state, such couplings were not observed.

Outlook

We have demonstrated that radioactive beams of heavy nuclei with $A \approx 220$ can be successfully accelerated with sufficient intensity to measure both even- and odd-order electric-multipole matrix elements with an accuracy of 10% or better. The extracted electric-quadrupole and electric-octupole moments are consistent with constant values over the range of measured angular momentum. Our data show that ^{220}Rn has weaker octupole collectivity than ^{224}Ra. We conclude that ^{219,221}Rn are likely to have smaller octupole-enhanced EDMs than ^{223,225}Ra, though more favourable Rn candidates may emerge from future studies of the low-lying structure of heavier isotopes. Comparing our data with predictions of the E3 strength from recent models, we find that the trend in octupole deformation extracted from the data presented here reveals detailed differences from some mean field predictions[16] and opposes the trend predicted by the cluster model[17]. Our findings for the comparisons with models should be confirmed by extending studies to other radioactive isotopes in the Rn and Ra chain. It is interesting to note that the Gogny HFB calculations[16] predict that Th and U isotopes with $N = 134$–136, already known to exhibit the characteristics of a rigid octupole shape[7,41], should have significantly enhanced E3 transition strengths (70 Weisskopf units); however, tests of this prediction await major developments in radioactive beam technology.

METHODS SUMMARY

In our experiments, the ^{220}Rn and ^{224}Ra produced by spallation diffused to the primary target surface and were then singly ionized ($q = 1^+$) in either an enhanced plasma ion-source[42] with a cooled transfer line (Rn) or a tungsten surface ion-source (Ra), accelerated to 30 keV, separated according to A/q, and delivered to a Penning trap, REXTRAP[43], at a rate of around 1.25×10^7 ions s^{-1} for ^{220}Rn and 4.4×10^7 ions s^{-1} for ^{224}Ra at the entrance. Inside the trap, the singly-charged ions were accumulated and cooled before allowing the ions to escape in bunches at 400 ms intervals into an electron-beam ion source, REXEBIS[43]. Here, the ions were confined for 400 ms in a high-density electron beam that stripped more electrons to produce a charge state of 52^+, extracted as 400 μs pulses before being mass-selected again according to A/q, and injected at 2.5 Hz into the REX linear post-accelerator. The level of isobaric impurity (for example, Fr) in the Ra beam was estimated to be below 1% by observing radioactive decays at the end of the beam line. For Rn, observation of contaminant decays was more difficult because of the small α-decay branching ratios to excited states, and only an upper limit of 5% could be obtained.

The GOSIA code performs a least-squares fit to the matrix elements between all known states coupled by electromagnetic operators, which are treated as free parameters. Although the fit is sensitive to the relative E1/E2 decay rates, E1 (and M1) excitation is negligible at the beam energies used and can be ignored. The magnitudes of the values of the starting parameters were chosen to be random, within reasonable limits. The fit was found to be insensitive to many of the matrix elements; these were either fixed or coupled to other matrix elements assuming the validity of the rotational model.

Received 30 January; accepted 13 March 2013.

1. Pospelov, M. & Ritz, A. Electric dipole moments as probes of new physics. *Ann. Phys.* **318,** 119–169 (2005).
2. Griffith, W. C. *et al.* Improved limit on the permanent electric dipole moment of ^{199}Hg. *Phys. Rev. Lett.* **102,** 101601 (2009).
3. Spevak, V., Auerbach, N. & Flambaum, V. V. Enhanced T-odd, P-odd electromagnetic moments in reflection asymmetric nuclei. *Phys. Rev. C* **56,** 1357–1369 (1997).
4. Dobaczewski, J. & Engel, J. Nuclear time-reversal violation and the Schiff moment of ^{225}Ra. *Phys. Rev. Lett.* **94,** 232502 (2005).
5. Ellis, J., Lee, J. & Pilaftsis, A. Maximal electric dipole moments of nuclei with enhanced Schiff moments. *J. High Energy Phys.* **2011,** 045 (2011).
6. Guest, J. R. *et al.* Laser trapping of ^{225}Ra and ^{226}Ra with repumping by room-temperature blackbody radiation. *Phys. Rev. Lett.* **98,** 093001 (2007).
7. Cocks, J. *et al.* Spectroscopy of Rn, Ra and Th isotopes using multi-nucleon transfer reactions. *Nucl. Phys. A* **645,** 61–91 (1999).
8. Dahlinger, M. *et al.* Alternating parity bands and octupole effects in ^{221}Th and ^{223}Th. *Nucl. Phys. A* **484,** 337–375 (1988).
9. Butler, P. A. & Nazarewicz, W. Intrinsic dipole moments in reflection-asymmetric nuclei. *Nucl. Phys. A* **533,** 249–268 (1991).
10. Nazarewicz, W. *et al.* Analysis of octupole instability in medium-mass and heavy nuclei. *Nucl. Phys. A* **429,** 269–295 (1984).
11. Möller, P. *et al.* Axial and reflection asymmetry of the nuclear ground state. *At. Data Nucl. Data Tables* **94,** 758–780 (2008).
12. Bonche, P., Heenen, P. H., Flocard, H. & Vautherin, D. Self-consistent calculation of the quadrupole-octupole deformation energy surface of ^{222}Ra. *Phys. Lett. B* **175,** 387–391 (1986).
13. Egido, J. & Robledo, L. Microscopic study of the octupole degree of freedom in the radium and thorium isotopes with Gogny forces. *Nucl. Phys. A* **494,** 85–101 (1989).
14. Rutz, K., Maruhn, J. A., Reinhard, P.-G. & Greiner, W. Fission barriers and asymmetric ground states in the relativistic mean-field theory. *Nucl. Phys. A* **590,** 680–702 (1995).
15. Engel, J., Bender, M., Dobaczewski, J., Jesus, J. H., d. & Olbratowski, P. Time-reversal violating Schiff moment of ^{225}Ra. *Phys. Rev. C* **68,** 025501 (2003).
16. Robledo, L. M. & Bertsch, G. F. Global systematics of octupole excitations in even-even nuclei. *Phys. Rev. C* **84,** 054302 (2011).
17. Shneidman, T. M., Adamian, G. G., Antonenko, N. V., Jolos, R. V. & Scheid, W. Cluster interpretation of properties of alternating parity bands in heavy nuclei. *Phys. Rev. C* **67,** 014313 (2003).
18. Buck, B., Merchant, A. C. & Perez, S. M. Negative parity bands in even–even isotopes of Ra, Th, U and Pu. *J. Phys. G* **35,** 085101 (2008).
19. Zamfir, N. V. & Kusnezov, D. Octupole correlations in the transitional actinides and the spdf interacting boson model. *Phys. Rev. C* **63,** 054306 (2001).

20. Frauendorf, S. Heart-shaped nuclei: condensation of rotational-aligned octupole phonons. *Phys. Rev. C* **77,** 021304 (2008).
21. Butler, P. A. & Nazarewicz, W. Intrinsic reflection asymmetry in atomic nuclei. *Rev. Mod. Phys.* **68,** 349–421 (1996).
22. Robledo, L. M. & Bertsch, G. F. Electromagnetic transition strengths in soft deformed nuclei. *Phys. Rev. C* **86,** 054306 (2012).
23. Wollersheim, H. J. *et al.* Coulomb excitation of ^{226}Ra. *Nucl. Phys. A* **556,** 261–280 (1993).
24. Voulot, D. *et al.* Radioactive beams at REX–ISOLDE: present status and latest developments. *Nucl. Instrum. Methods B* **266,** 4103–4107 (2008).
25. Eberth, J. *et al.* MINIBALL A Ge detector array for radioactive ion beam facilities. *Prog. Part. Nucl. Phys.* **46,** 389–398 (2001).
26. Ostrowski, A. *et al.* CD: A double sided silicon strip detector for radioactive nuclear beam experiments. *Nucl. Instrum. Methods A* **480,** 448–455 (2002).
27. Bell, R. E., Bjornholm, S. & Severiens, J. C. Half lives of first excited states of even nuclei of Fm, Ra, Th, U, and Pu. *Kgl. Danske Vid. Selsk. Mat.-Fys. Medd.* **32,** 1–48 (1960).
28. Neal, W. R. & Kraner, H. W. Mean lives of excited rotational states of heavy even-even nuclei. *Phys. Rev.* **137,** B1164–B1174 (1965).
29. Liang, C. F., Paris, P., Ruchowska, E. & Briancon, C. A new isotope $_{85}{}^{220}At_{135}$. *J. Phys. G* **15,** L31–L33 (1989).
30. Artna-Cohen, A. Nuclear data sheets for A = 224. *Nucl. Data Sheets* **80,** 227–262 (1997).
31. Cline, D. Quadrupole and octupole shapes in nuclei. *Nucl. Phys. A* **557,** 615–634 (1993).
32. Nazarewicz, W. & Tabor, S. L. Octupole shapes and shape changes at high spins in the Z ~58, N ~88 nuclei. *Phys. Rev. C* **45,** 2226–2237 (1992).
33. Ibbotson, R. W. *et al.* Quadrupole and octupole collectivity in ^{148}Nd. *Nucl. Phys. A* **619,** 213–240 (1997).
34. Leander, G. A. & Chen, Y. S. Reflection-asymmetric rotor model of odd A ~ 219–229 nuclei. *Phys. Rev. C* **37,** 2744–2778 (1988).
35. Riley, L. A. *et al.* Conversion electron-γ coincidences and intrinsic reflection asymmetry in ^{219}Ra. *Phys. Rev. C* **62,** 021301 (2000).
36. Ackermann, B. *et al.* Level structure of ^{217}Rn and ^{221}Ra investigated in the alpha-decay ^{225}Th → ^{221}Ra → ^{217}Rn. *Z. Phys. A* **332,** 375–381 (1989).
37. Nosek, D., Sheline, R. K., Sood, P. C. & Kvasil, J. Microscopic structures of parity doublets in the ^{151}Pm, ^{153}Eu and ^{155}Eu nuclei. *Z. Phys. A* **344,** 277–283 (1993).
38. Rząca-Urban, T. *et al.* Reflection symmetry of the near-yrast excitations in ^{145}Ba. *Phys. Rev. C* **86,** 044324 (2012).
39. Poynter, R. J. *et al.* Observation of unexpectedly small E1 moments in ^{224}Ra. *Phys. Lett. B* **232,** 447–451 (1989).
40. Goriely, S., Hilaire, S., Girod, M. & Péru, S. First Gogny-Hartree-Fock-Bogoliubov nuclear mass model. *Phys. Rev. Lett.* **102,** 242501 (2009).
41. Greenlees, P. T. *et al.* First observation of excited states in ^{226}U. *J. Phys. G* **24,** L63–L70 (1998).
42. Penescu, L., Catherall, R., Lettry, J. & Stora, T. Development of high efficiency versatile arc discharge ion source at CERN ISOLDE. *Rev. Sci. Instrum.* **81,** 02A906 (2010).
43. Wolf, B. H. *et al.* First radioactive ions charge bred in REXEBIS at the REX-ISOLDE accelerator. *Nucl. Instrum. Methods Phys. Res. B* **204,** 428–432 (2003).
44. Martin, M. J. Nuclear data sheets for A = 208. *Nucl. Data Sheets* **108,** 1583–1806 (2007).
45. Bemis, C. E. *et al.* E2 and E4 transition moments and equilibrium deformations in the actinide nuclei. *Phys. Rev. C* **8,** 1466–1480 (1973).
46. Baktash, C. & Saladin, J. X. Determination of E2 and E4 transition moments in ^{232}Th. *Phys. Rev. C* **10,** 1136–1139 (1974).
47. McGowan, F. K. *et al.* Coulomb excitation of vibrational-like states in the even-A actinide nuclei. *Phys. Rev. C* **10,** 1146–1155 (1974).
48. McGowan, F. & Milner, W. Coulomb excitation of states in ^{232}Th. *Nucl. Phys. A* **562,** 241–259 (1993).
49. Singh, S., Jain, A. & Tuli, J. K. Nuclear data sheets for A = 222. *Nucl. Data Sheets* **112,** 2851–2886 (2011).
50. Artna-Cohen, A. Nuclear data sheets for A = 228. *Nucl. Data Sheets* **80,** 723–786 (1997).

Acknowledgements The support of the ISOLDE Collaboration and technical teams is acknowledged. This work was supported by the following Research Councils: STFC (UK), BMBF(Germany; 05P12RDCIA, 06DA9036I, 06KY9136I and 06KY205I), HIC for FAIR (Germany), FWO-Vlaanderen (Belgium), Belgian Science Policy Office (IAP-BriX network P7/12), Academy of Finland (contract no. 131665), DOE (US; DE-AC52-07NA27344 and DE-FG02-04ER41331), NSF (US), MICINN (Spain; FPA2009-08958 and FIS2009-07277), Consolider-Ingenio 2010 Programmes (Spain; CPAN CSD2007-00042 and MULTIDARK CSD2009-00064), Polish Ministry for Science and Higher Education (grant no. 589/N-G-POOL/2009/0), EC via I3-EURONS (FP6 contract no. RII3-CT-2004-506065), MC Fellowship scheme (FP7 contract PIEF-GA-2008-219175) and IA-ENSAR (FP7 contract 262010).

Author Contributions Instrument set-up: M.A., C.B., A.B., T.D., H.D.W., L.P.G., J.K., J.P., P.R., M. Seidlitz, B.S., M.J.V. and N.W. DAQ and on-line analysis: A.B., L.P.G., R.L. and N.W. Data analysis and interpretation: L.P.G., P.A.B., D.C., A.B.H., M. Scheck and M.Z. REX development and set-up: F.W., D.V. and J.C. Primary target: T.S. Preparation of manuscript: P.A.B., L.P.G., T.C., A.B., D.G.J., Th.K., J.P., P.R., M. Scheck, P.V.D. and N.W. Theoretical interpretation: L.M.R. All authors except L.M.R. took part in the experiments.

Author Information Reprints and permissions information is available at www.nature.com/reprints. The authors declare no competing financial interests. Readers are welcome to comment on the online version of the paper. Correspondence and requests for materials should be addressed to P.A.B. (peter.butler@liverpool.ac.uk).